

Error Diagrams and Temporal Correlations in a Fracture Model with Characteristic and Power-Law Distributed Avalanches

Yamir Moreno,^{1,2} Miguel Vázquez-Prada,¹ Javier B. Gómez,³ and Amilio F. Pacheco^{1,2}

¹*Departamento de Física Teórica, Universidad de Zaragoza, Zaragoza 50009, Spain*

²*Instituto de Biocomputación y Física de Sistemas Complejos,
Universidad de Zaragoza, Zaragoza 50009, Spain*

³*Departamento de Ciencias de la Tierra, Universidad de Zaragoza, Zaragoza 50009, Spain*

(Dated: October 20, 2019)

Forecasting failure events is one of the most important problems in fracture mechanics and related sciences. In this paper, we use the Molchan scheme to investigate the error diagrams in a fracture model which has the notable advantage of displaying two completely different regimes according to the heterogeneity of the system. In one regime, a characteristic event is observed while for the second regime a power-law spectrum of avalanches is obtained reminiscent of self-organized criticality. We find that both regimes are different when predicting large avalanches and that, in the second regime, there are non-trivial temporal correlations associated to clustering of large events. Finally, we extend the discussion to seismology, where both kinds of avalanche size distributions can be seen.

PACS numbers: 46.50.+a, 91.45.Vz, 62.20.Mk

I. INTRODUCTION

The fracture of heterogeneous materials has been the subject of intensive research since many years ago and is one of the oldest concerns of science [1]. This is not only due to the evident practical and potential profits, but also because the understanding of fracture processes at a basic level has shed light on other phenomena like earthquake occurrence [2, 3]. Relatively simple models such as random resistor networks [4], beam networks [5], spring-block models [6, 7, 8] and the so-called Fibre Bundle Models (FBMs) [1, 3, 9, 10, 11, 12] have guided our way to more complex models of fracture. To date, we actually know many of the failure properties and its dynamics. Yet, the range of phenomena associated with fracture has not been cast into a definite physical and theoretical treatment. Some years ago, there was a burst of activity in what today we know as self-organized criticality [13, 14], a theoretical framework that was soon applied to the study of fracture processes and avalanche like phenomena in disordered system. Soon afterwards, some interesting claimings were put out as, for example, the suggestion that the earth's crust is in a self-organized critical state, being the Gutenberg-Richter (GR) law [15] for the frequency of earthquakes with a given magnitude a result of this self-organization process [16, 17, 18].

From a more practical point of view, perhaps the most important concern related to fracture processes that remains unsolved is their predictability [19]. One is interested in knowing not only under what circumstances a material will fail or how the distribution of energy releases looks like, but also *when* a material will break down or an event of a given magnitude (usually we are interested in largest quakes) will take place. This problem is far from being solved and different approaches have been adopted in order to increase the prediction power of actual methods [19]. For instance, in seismicity, there

is an unavoidable degree of arbitrariness in classifying earthquakes. When a relative big earthquake occurs, it can be either a foreshock of a larger subsequent event, an aftershock of a preceding large quake or the mainshock itself. Thus there is no way to differentiate these events in real time and many algorithms and methods are useless from a practical point of view as they perform only *a posteriori*. However, regardless of how a big event may be classified, the forecasting of large quakes is the main goal to be achieved. This is the type of challenge that we face here.

In this paper, we analyze a dissipative fibre bundle model of fracture with only one parameter that characterizes the heterogeneity degree of the system [20]. Noticeably, the model exhibits two very distinct failure regimes obeying different avalanche size distributions. This allows the study of the occurrence of large avalanches, for the two phases, within the same model. In one of these regimes, the avalanche size distribution shows a power law regime for small events separated by a gap from the larger events, which are of the order of the system size. This regime is reminiscent of the characteristic earthquake behavior found in some seismic faults [21, 22]. On the other hand, in the second regime, the system self-organizes into a critical state characterized by a unique power law avalanche distribution similar to the GR law. Following the Molchan method [23] we compute the error diagrams that quantify the forecasting of large cascade events and analyze their correlations in time. Our results and model might apply to the study of earthquake occurrence where one may actually have both failure regimes.

II. FAILURE MODEL

The basic ingredients and main features of the model to be inspected are as follows [20]:

1. A set of N elements is located on the sites of a supporting square lattice of linear length L . Each element represents a fibre, or in general terms, a small volume fraction of the material under study.
2. To each element i , one assigns a random threshold strength $\sigma_{i_{th}}$ taken from a probability distribution. The threshold values represent the maximum load each of the elements can support before failure occurs. We use henceforth a Weibull distribution to assign the failure thresholds assuming a reference load $\sigma_0 = 1$ [20].
3. At each time step, the load on the system is increased by calculating the minimum load required for one element to break and adding this amount to all the elements, *i.e.*, $\sigma_i \rightarrow \sigma_i + \nu$, where $\nu = \min\{\sigma_{i_{th}} - \sigma_i\}$.
4. Once the load acting on an element surpasses its failure threshold, it fails and the load it bears is equally redistributed among *all* the elements of the set *irrespective* of their state. This amounts to a global fibre bundle version where long range interactions are assumed.
5. The fraction of load that would correspond to already failed elements is simply dissipated so that the model is *nonconservative*. Moreover, the degree of dissipation depends on both the avalanche size and its internal structure [20].
6. The redistribution of load to non-broken fibres may trigger more failure events. In such a case, step 4 is repeated until the system reaches a state where all the elements support a load below their respective threshold values.
7. When an avalanche has come to an end, the external driving, step 3, is repeated and the elements that have been broken in the preceding avalanche are healed assigning to them new random strengths and a load equal to zero.

The model is thus constructed by implicitly taking into account some general properties of any fracture process. Two ingredients of our model are worth mentioning. First, we assume dissipation through broken elements. This amounts to consider that the energy dissipated during a given fracture event is proportional to the size and the duration of that event. Besides, we incorporate healing only after an avalanche has ended because when the ongoing avalanche is developing, the elements have no time for healing and broken regions should not accumulate stress in that time interval.

There are two different time scales in the model [20]. One refers to the external driving of the system and defines the *natural* time interval between failure events. We measure the time elapsed until a given event k as the sum

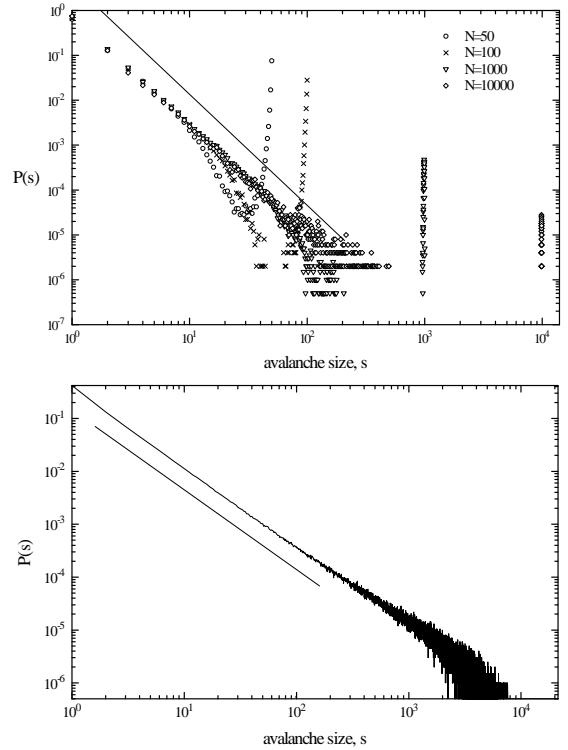


FIG. 1: Distributions of avalanche sizes for the two failure regimes that characterize the model. The upper part corresponds to a system that can be regarded as fairly homogeneous ($\rho = 4$) while the lower figure is obtained for a more heterogeneous system made up of $N = 50000$ fibres ($\rho = 2$). The solid lines have slopes -2.5 and -1.5 respectively. After [20].

of the incremental amounts of load added at every external loading of the system prior to the event k . This definition of time assumes that the rate at which the system is loaded can be considered constant, and hence that ν is linearly proportional to the time elapsed since the last event. This approximation holds, for example, in seismology. The second time scale of the process quantifies the avalanche lifetimes, and it is measured as lattice updates. That is, we consider the avalanches to be instantaneous with respect to the external driving and separated by an interval of time whose length is proportional to the amount of energy added to the system during the last external input.

The iteration of the rules sketched above leads the system to two different behaviors depending on the level of heterogeneity assumed when assigning the threshold values [20]. Figure 1 shows the distributions of avalanche sizes, $P(s)$, for the two failure regimes of the model. The upper panel shows the pattern typical of characteristic quakes which are distributed quasi-periodically in time. This regime, where there are large fluctuations of the load on the system, is obtained when the bundle of fibres is homogeneous (large values of the Weibull index

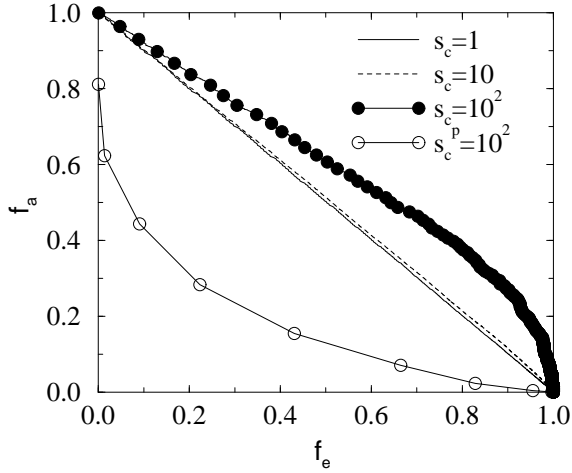


FIG. 2: Error diagrams for the two failure regimes. Open circles represent the trade-off between f_a and f_e when the system can be regarded as homogeneous ($\rho = 4$ and $N = 100$ elements). Full circles have been obtained for a system made up of $N = 10^4$ fibres and $\rho = 2$; the dashed line shows the effects of reducing the target threshold, s_c ; the solid line corresponds to the case in which avalanches of any size are forecasted (equivalent to a random process).

ρ), that is, when the deviation of the thresholds from a mean value is not large. Note that as the system size is increased, large events are better resolved and there are no intermediate avalanches.

A richer and more complex behavior is found when the system departs from homogeneity and the bundle of fibres gets heterogeneous (small values of ρ). In this case, irrespective of the system size, a power law distribution for the avalanche sizes is obtained. This is depicted in the lower panel of Figure 1 for $\rho = 2$ and $N = 50000$ fibres. As we shall see in the next section, the quasi-periodic nature of the first regime makes the forecasting of large avalanches feasible and eventually, for large system sizes (strictly speaking, in the thermodynamic limit), one can always forecast such events with no errors. This is not anymore the case when the system can be regarded as heterogeneous, as non-trivial temporal correlations and clustering of large events come into play making the forecasting of catastrophic avalanches a hard task.

III. ERROR DIAGRAMS AND TEMPORAL CORRELATIONS

In order to inspect whether or not we would be able to predict large events, we first compute the errors diagrams for both failure regimes. They are a quantitative measure of the success in forecasting the occurrence of a given event and were introduced in seismology several years ago by Molchan [23] with the aim of evaluating different algorithms for large earthquakes prediction, and



FIG. 3: Time sequence of events, in a model with $\rho = 2$, with sizes equal to or greater than s . The time intervals have been rescaled so that the density of points is the same in both series. The system consist of $N = 50000$ elements. Note the clustering of large quakes ($s > 10^3$).

subsequently used by other authors [19, 24, 25, 26].

An error diagram requires the identification of a target to be forecasted using alarms. Then, one plots the trade-off between the fraction of target events that were not predicted, f_e , and the fraction of time that the alarm was active, f_a . Ideally, one would like to get the smallest number of failures to predict at the minimum duration of the alarms. Points close to the origin of an error diagram represent the best predictions. Hence, the efficiency of a given forecasting algorithm is measured by how fast f_e decreases when increasing f_a . In practice, one switches on the alarm at a given time interval τ after the preceding event. If $\tau = 0$, the fraction of failures to predict is zero, but the fraction of alarm time is 1. On the contrary, if τ is equal to (or greater than) the time interval between two successive events, $f_a = 0$ but $f_e = 1$. In this way, the result of a completely random (Poissonian) process is a diagonal line.

Let us now construct the error diagrams for each of the regimes of the fracture model under study. First, we define the targets as the large avalanches whose sizes exceed a given threshold s_c and fix the time interval τ at which the alarms are switched on after every large failure event. By varying the length of τ and computing the fractions of failures to forecast and of alarm times, $f_e(\tau)$ and $f_a(\tau)$ respectively, the error diagrams shown in Fig. 2 are obtained, where the dependency on τ has been eliminated. The figure clearly illustrates how different with respect to successful forecast the two failure regimes are. Open circles represent the results of the algorithm when applied to the prediction of characteristic events in the parameter region when the system is homogeneous. Here, target events occur quasi-periodically and thus setting τ close to the mean time interval between large avalanches

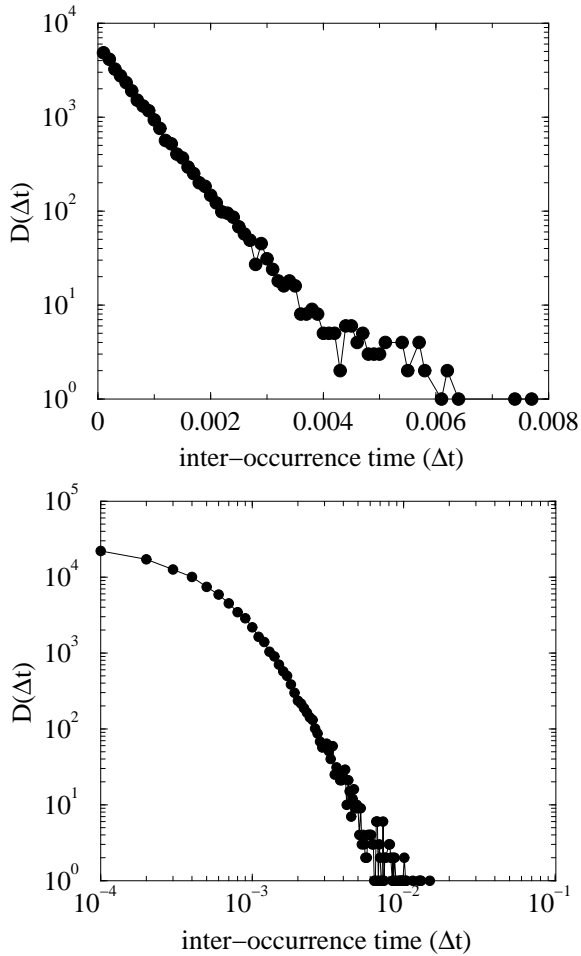


FIG. 4: Distributions of inter-occurrence time Δt for a system of $N = 10^4$ elements and $\rho = 2$. The upper figure is in linear-log scale so that the distribution of Δt follows an exponential law when s_c is small ($s_c > 10$). The lower panel corresponds to s_c equal to or greater than 10^2 so that only large avalanches are taken into account. In this case, the inter-occurrence times are power law distributed.

ensures a successful prediction with a minimum of alarm time. For example, one can choose τ so that $f_a \approx 0.3$ and $f_e \approx 0.2$, a rather good forecasting. Besides, increasing the system size improves the prediction of characteristic events since there appears a gap between small and large events making the definition of targets less noisy. In this case, the error diagram approaches a delta function at the origin as large failure events occur almost periodically in time.

On the contrary, when the system gets heterogeneous, the error diagram is worse than a random prediction since f_a is always above f_e (full circles). Here, we consider an avalanche as a target when its size falls on the edge of the distribution $P(s)$, where finite size effects appear. Reducing the target thresholds move the error diagram close to the diagonal line. In fact, the occurrence of an event of any size is a random process as can be observed in the figure when the threshold is set equal to 1.

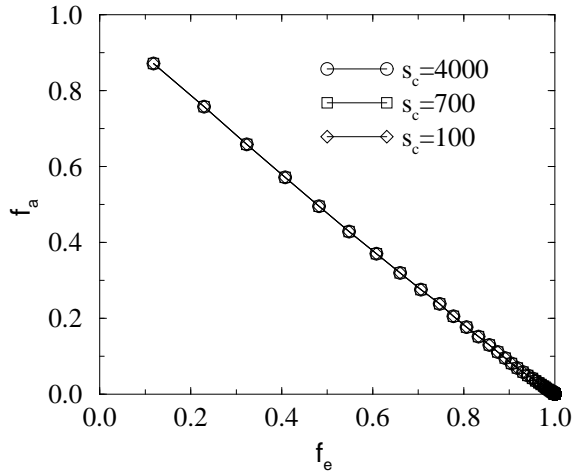


FIG. 5: Error diagrams of the BTW model for different values of the target thresholds. Note that irrespective of s_c , the forecast is completely random in agreement with the fact that the BTW model does not show any kind of temporal correlations. The system size is $N = 75 \times 75$.

Another interesting information that can be extracted from the error diagrams for the second regime is the existence of some degree of non-trivial temporal correlations. The departure from a random process when the target threshold is increased indicates that large events show clustering in time. This is clearly appreciated in Fig. 3, where two sequences of quakes for a system made up of $N = 50000$ elements and $\rho = 2$ has been represented. The upper series is the occurrence of events with sizes equal to or greater than 10^2 while the lower sequence is obtained when s_c is equal to 10^3 (upper limit for events not affected by finite-size effects).

We also present in Fig. 4 the distribution of inter-occurrence time Δt for two values of the target thresholds. We see that when s_c is increased so that only large avalanches are taking into account, the distribution $D(\Delta t)$ radically changes from an exponential decay (typical of a random process) to a decaying power law. This is in perfect agreement with the error diagrams previously shown and provides further evidence that small avalanches are not correlated while large ones are. Without providing a figure, we point out that the distribution of inter-occurrence time for the first failure regime is a well-behaved function with a clear mean value and a dispersion that decreases as the system gets larger.

IV. DISCUSSION AND CONCLUSIONS

The results shown in the preceding section indicate that the clustering of large avalanches makes the prediction of such events a hard task. The shape of the error diagrams and the high rate of prediction failures can be understood by noticing that the average inter-occurrence time between *all* large events is not a useful reference in

this case. Two other quantities seem to be more fundamental: the *inter-cluster* average time defined as the time interval between clusters of large avalanches and the mean *intra-cluster* time defined as the time between large events *within* the same cluster. Since the former is much larger than the latter, the fraction of failures to predict is raised when τ is large. On the other hand, setting τ too small to match the *intra-cluster* time produces a significant increment of f_a . Thus both phenomena contribute to the error diagrams in such a way that the forecasting is worse than a random prediction.

The clustering of large events is due to the way in which energy is dissipated and not to the power-law nature of the avalanche size distribution. The average inter-occurrence time between large quakes can be considered as a measure of the buildup time for correlations in the system. When a series of big cascades occurs, the system ends up in a state where most of the elements are unloaded and a significant input of energy (or a large time interval) is needed in order to start another series. In other words, the way in which energy is dissipated creates stress correlations giving rise on its turn to the observed clustering. This does not hold anymore when avalanches of smaller sizes are considered. In this case, the occurrence of a small avalanche does not significantly alter the state of the system. A small event can not influence the occurrence of any event at short times.

The same kind of temporal correlations is seen in other models displaying self-organized criticality. This is the case of the Olami, Feder and Christensen (OFC) spring-block model for earthquakes [7, 8]. They found some years ago that non-trivial temporal correlations of the sort obtained here show up when the model is made non-conservative. By calculating the coefficient of variation, it was shown that large earthquakes show clustering while small ones are uncorrelated in time. Besides, when the model is conservative, neither spatial nor temporal correlations were found [8]. The fact that dissipation appears to be a basic ingredient for a model to show correlations in time and/or space is corroborated in Fig. 5, where the error diagrams for the original Bak, Tang and Wiesenfeld (BTW) model [13, 14] are depicted. As can be clearly seen in the figure, the model can not be distinguished

from a random process with regard to its predictability. Changing the target thresholds does not improve the forecasting. Thus, in this model, small avalanches and large ones are completely equivalent and all correlations are ruled out.

We would like to remark that the results obtained in this paper may be applied to the study of earthquake occurrence. One of the few well-known facts in seismology is the clustering of earthquakes in time and space. While small earthquakes seem to be uncorrelated [27], large earthquakes display strong clustering [28, 29]. On the other hand, by tuning a single parameter in our model, one moves from a characteristic earthquake scenario to a regime where the avalanche sizes are power law distributed (GR law). The possibility of exploring such different regimes within the same model is another motivation for further research in this direction [30]. In this sense, our results and model might be useful in the search of more complex tools for earthquake modeling and forecasting.

Summing up, we have analyzed a fracture model with interesting temporal correlations. The results presented seem to support the idea that models aimed at modeling real earthquakes should incorporate some kind of dissipation and self-organization. On the other hand, the clustering of large quakes does not help to improve the predictability of devastating events since two relevant time scales come into play. It might be interesting to compute the error diagrams with a tunable alarm time in such a way that one can better resolve series of large events and periods of stasis.

Acknowledgments

Y. M. acknowledges financial support from the Secretaría de Estado de Educación y Universidades (Spain, SB2000-0357). M. V-P. is supported by the Ph.D grant B037/2001 of the DGA. This work has been partially supported by the Spanish DGICYT project BFM2002-01798.

[1] H. J. Herrmann, and S. Roux, (Eds), *Statistical Models for the Fracture of Disordered Media* (North Holland, Amsterdam, 1990), and references therein.
[2] D. L. Turcotte, *Fractals and Chaos in Geology and Geophysics*. 2nd ed (Cambridge University Press, Cambridge, New York, 1997).
[3] D. Sornette, *Critical Phenomena in Natural Sciences*, (Springer-Verlag, New York, 2000).
[4] L. de Arcangelis, S. Redner, and H. J. Herrmann, *J. Phys. (Paris)* **46**, L585 (1985).
[5] S. Roux, and E. Guyon, *J. Phys. (France) Lett.* **46**, L999 (1985).
[6] R. Burridge, and L. Knopoff, *Bull. Seismol. Soc. Am.* **57**, 341 (1967).
[7] Z. Olami, H. J. Feder, and K. Christensen, *Phys. Rev. Lett.* **68**, 1244 (1992).
[8] K. Christensen, and Z. Olami, *J. Geophys. Res.* **97**, 8729 (1992).
[9] H. E. Daniels, *Proc. R. Soc. London, Ser. A* **183**, 404 (1945).
[10] W. I. Newman, D. L. Turcotte, and A. M. Gabrielov, *Phys. Rev. E* **52**, 4827 (1995).
[11] P. C. Hemmer, and A. Hansen, *J. Appl. Mech.* **59**, 909 (1992).

- [12] Y. Moreno, J. B. Gómez, and A. F. Pacheco, *Phys. Rev. Lett.* **85**, 2865 (2000).
- [13] P. Bak, C. Tang, and K. Wiesenfeld, *Phys. Rev. Lett.* **59**, 381 (1987).
- [14] P. Bak, C. Tang, and K. Wiesenfeld, *Phys. Rev. A* **38**, 364 (1988).
- [15] G. Gutenberg, and C. F. Richter, *Ann. Geophys.* **9**, 1 (1956).
- [16] P. Bak, and C. Tang, *J. Geophys. Res.* **94**, 15635 (1989).
- [17] D. Sornette, and A. Sornette, *Europhys. Lett.* **9**, 197 (1989).
- [18] K. Ito, and M. Matsuzaki, *J. Geophys. Res.* **95**, 6853 (1990).
- [19] V. Keilis-Borok, *Annu. Rev. Earth Planet. Sci.* **30**, 1 (2002).
- [20] Y. Moreno, J. B. Gómez, and A. F. Pacheco, *Physica A* **274**, 400 (1999).
- [21] S. G. Wesnousky, *Bull. Seismol. Soc. Am.* **84**, 1940 (1994).
- [22] K. Sieh, *Proc. Natl. Acad. Sci. USA* **93**, 3764 (1996).
- [23] G. M. Molchan, *Pure Appl. Geophys.* **149**, 233 (1997).
- [24] W. I. Newman, and D. L. Turcotte, *Nonlin. Proc. Geophys.* **9**, 1 (2002).
- [25] A. Helmstetter, and D. Sornette, *e-print* cond-mat/0208597 (2002).
- [26] M. Vázquez-Prada, Á. González, J. B. Gómez, and A. F. Pacheco, unpublished (2003).
- [27] A. C. Johnston, and S. J. Nava, *J. Geophys. Res.* **90**, 6737 (1985).
- [28] Y. Y. Kagan, and D. D. Jackson, *Geophys. J. Int.* **104**, 117 (1991).
- [29] M. S. Mega, P. Allegrini, P. Grigolini, V. Latora, L. Palatella, A. Rapisarda, and S. Vinciguerra, *Phys. Rev. Lett.*, in press. Also *e-print* cond-mat/0208597 (2002).
- [30] Models able to pass from the GR to a characteristic earthquake behavior are not found very often in the literature. One of such models was proposed in [31], where the concept of configurational entropy is used to argue the existence of the two regimes. Our model also suggests that these two behaviors can be recognized when the degree of heterogeneity of the faults under study are different. See also [32] for a further test of the configurational entropy hypothesis.
- [31] K. Dahmen, D. Ertas, and Y. Ben-Zion, *Phys. Rev. E* **58**, 1494 (1998).
- [32] M. Vázquez-Prada, Á. González, J. B. Gómez, and A. F. Pacheco, *Nonlin. Proc. Geophys.* **9**, 513 (2002).